

Particle flows around an intruder

Satoshi Takada*

*Institute of Engineering, Tokyo University of Agriculture and Technology,
2-24-16, Naka-cho, Koganei, Tokyo 184-8588, Japan*

Hisao Hayakawa

*Yukawa Institute for Theoretical Physics, Kyoto University,
Kitashirakawa Oiwakecho, Sakyo-ku, Kyoto 606-8502, Japan*

(Dated: November 6, 2019)

Particle flows injected as a beam and scattered by an intruder are numerically studied. We find a crossover of the drag force from Epstein's law to Newton's law depending on the ratio of the speed to the thermal speed. These asymptotic laws can be reproduced by a simple analysis of a collision model between the intruder and the particle flows. The crossover from Epstein's law to Stokes' law is also reproducible for the low speed regime as a time evolution of the drag force caused by beam particles. We also show the existence of weak turbulent-like behavior of the particle flows behind the intruder with the aid of the second invariant of the velocity gradient tensor and the relative mean square displacement for the high speed regime.

I. INTRODUCTION

To know fluid flows around an intruder depending on the Reynolds number is a fundamental problem [1, 2]. When the flow speed is low, the drag force acting on a spherical intruder obeys Stokes' law in which the drag is proportional to the speed, the viscosity of the fluid, and the radius of the intruder. Whereas the drag force satisfies Newton's law for the high Reynolds number, in which the drag is proportional to the square of the moving speed and the cross section.

We believe that the drag force still satisfies Stokes' law even for low speed molecules [3–7]. It is known that Stokes' law can be used only for systems in the zero Knudsen number limit, the ratio of the mean free path to the intruder size [8–13]. The correction to Stokes' drag for rarefied gases in the low Knudsen number is theoretically confirmed by the kinetic theory [8–13]. Whereas the drag force acting on slowly moving intruders in the large Knudsen number satisfies Epstein's law [14, 15]. It is known that the drag law depends on the distance from the boundary of a container through a simulation [3] and a theory by fluid mechanics [16]. We also note that the Kármán vortices have already been observed in molecular dynamics (MD) simulations [7, 17, 18].

There are various experimental and numerical studies on the drag forces acting on an intruder in granular flows [19–32]. A variety of velocity dependences of the drag force are reported, depending on the protocols of experiments and simulations. Granular jet experiments [33, 34] and simulations [34–36] suggest that the granular jet flows can be approximated by a perfect fluid model [34, 35].

In this paper, we numerically study the drag force acting on a spherical intruder in particle flows by controlling the ratio of the injected speed of the particles to the thermal speed which is proportional to the sound speed in

terms of the MD. We characterize a weak turbulent-like behavior of particle flows behind the intruder with the aid of the second invariant of the velocity gradient tensor and the relative mean square displacement. We also characterize the scattering of particles by the intruder using the angular distribution function of scattered particles.

The organization of this paper is as follows: In the next section, we explain our model and setup of our study. In Sec. III, we present the results of our simulation, which consists of four parts. In the first part we show the crossover from Epstein's drag law to Newtonian drag law depending on the ratio of the colliding speed to the thermal speed. In the second part, we discuss how results depend on the boundary condition on the surface of the intruder. In the third part, we illustrate the existence of a crossover from Epstein's flow to Stokes' flow as a time evolution of the drag law caused by a particles' flow. In the last part, we demonstrate the existence of a weak turbulence-like behavior of the flow behind the intruder in which the relative distance between two colliding particles is super-ballistic. We also discuss the angle distribution of scattered particles by the intruder. In Secs. IV and V, we discuss and conclude our results.

II. MODEL

In this section, let us explain our model and setup of our simulation. The system consists of two parts: one is a fixed intruder and another is the mobile particles as shown in Fig. 1. The intruder is made by one core particle whose diameter is D_c . In most of cases, the intruder is covered by N_s identical particles whose diameters are d on the surface of the core particle. We examine three sizes of the intruders as $(D_c/d, N_s) = (5, 144)$, $(13, 744)$, and $(28, 1600)$. The diameter of the intruder is given by $D = D_c + 2d$ in this case. We also examine the case of $N_s = 0$ i. e. $D = D_c$ in Sec. III.2. Then, we find that the results are almost independent of the boundary condi-

* e-mail: takada@go.tuat.ac.jp

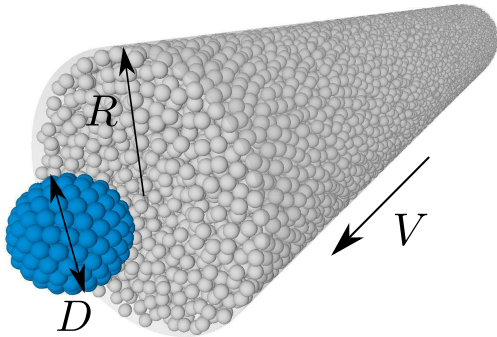


FIG. 1. A snapshot of the initial configuration of the system for $\phi = 0.40$, $D = 7d$, and $R = 10d$.

tion on the surface of the intruder. The intruder is fixed at the origin, which has infinitely large mass. We simulate systems containing $N = 30000$, 101250 , and 810000 monodisperse mobile particles whose mass and diameter are m and d , respectively. Throughout this paper, collisions between particles are always assumed to be elastic. We examine various initial volume fractions of beam particles ranged from $\phi = 0.20$ to 0.55 . Before starting our simulation, the mobile particles are thermalized with the temperature T , and are moved with the translational speed V . The equation of motion of i -th particle is given by $m d^2 \mathbf{r}_i / dt^2 = \sum_j \mathbf{F}_{ij}$ with the interparticle force $\mathbf{F}_{ij} = \Theta(d - r_{ij})k(d - r_{ij})$, where we have introduced $r_{ij} = |\mathbf{r}_i - \mathbf{r}_j|$, the spring constant k , and the step function $\Theta(x)$, i. e., $\Theta(x) = 1$ for $x \geq 0$ and $\Theta(x) = 0$ otherwise. Initially, we confine the mobile particles in tubes whose radii are $R = 10d$ for $D_c = 5d$ and $13d$ and $R = 30d$ for $D_c = 28d$, respectively. We assume that the interactive force between the wall of the tube and the particles is identical to the interparticle force. The used parameters are listed in Table I.

TABLE I. The set of used parameters.

D_c/d	N_s	N	R/d
5	144	30000	10
13	744	101250	15
28	3365	810000	30

When the mobile particles collide with the intruder, we examine two cases for the reflection: one is the random reflection of the angle with the temperature T_w , and another is the simple collision rule according to the equation of motion. Here, we set $T_w = T$ for simplicity for the former condition. We also examine two cases for the systems behind the intruder: one is a free scattering case, and another is a confined case, where the scattered particles are still confined in the tube.

In the following, we use the time-averaged drag force in a steady state, and fix the speed $V = 1.0 \times 10^{-1} d \sqrt{k/m}$. We have verified that the results of our simulation for $V = 1.0 \times 10^{-1} d \sqrt{k/m}$ are consistent with those of the hard-core particles.

III. RESULTS

In this section, we present the results of our simulations. In Sec. III.1, we show the drag force against the translational speed as a crossover from Epstein's law to Newtonian law depending on the ratio of the colliding speed to the thermal speed. In Sec. III.2, we investigate whether the geometry of the intruder affects the drag law. In Sec. III.3, we present the crossover for low speed regime. In Sec. III.4, we characterize the flows behind the intruder.

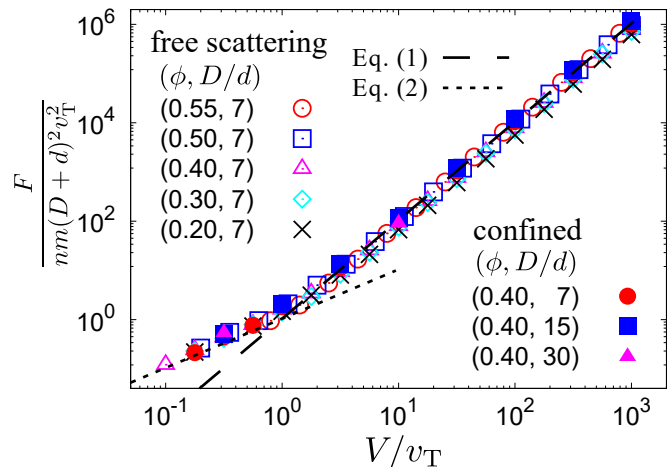


FIG. 2. Plots of the drag force against the normalized speed V/v_T for the free scattering and the confined cases for various fractions ϕ and intruder sizes D . The dashed and dotted lines represent the collision models (1) and (2), respectively.

III.1. Crossover of the drag force from Epstein's law to Newtonian law

We present the results of our simulation of the drag force acting on the intruder against the normalized colliding speed by the thermal speed $v_T \equiv \sqrt{2T/m}$ for both the free scattering and the confined cases (see Fig. 2). Because the drag force is determined from the impulses by collisions of particles in front of the intruder, the drag force is unchanged whether particles flow is confined or not behind the intruder. We note that our obtained drag forces are proportional to $(D + d)^2$, i. e., the collision cross section [21, 37]. The drag force is proportional to the square of the speed for $V/v_T \gg 1$, while it is proportional to V/v_T for $V/v_T \ll 1$. The former can be understood by a simple collision model. Because each momentum change in the flow direction for a collision is

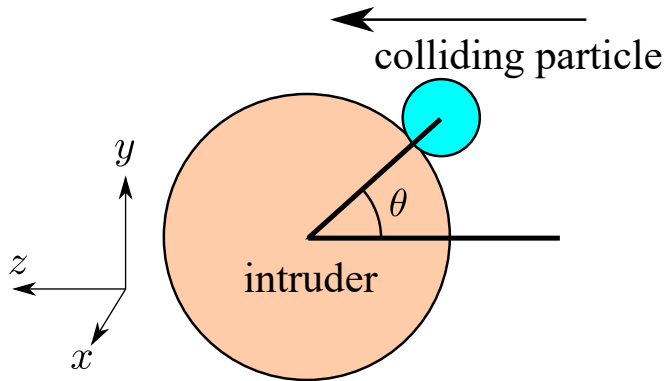


FIG. 3. Definition of the angle θ between the intruder and the colliding particle. The arrow indicates the flow direction. We define z -axis as the flow direction.

$\Delta p_{\parallel} = 2mV \cos^2 \theta$ where θ is the angle between the intruder and the colliding particle as shown in Fig. 3, and the collision frequency is $\Omega_c = (\pi/4)n(D+d)^2V$ with the number density $n = 6\phi/(\pi d^3)$ [21], the force acting on the intruder is given by

$$F = \int_0^{\pi} \sin^2 \theta d\theta d\phi \Delta p_{\parallel} \Omega_c = \frac{\pi}{3} nm(D+d)^2 V^2, \quad (1)$$

which agrees well with the simulation for $V > v_T$ (see Fig. 2). This is the simple Newtonian drag law for high speed regime.

Whereas the front of the beam of mobile particles diffuses before the collision for $V/v_T \ll 1$ as shown in Fig. 4(a). This expansion speed of the diffusive front is approximately given by $V_p = \sqrt{V}v_T$ as shown in Fig. 4(b). When we replace V in Eq. (1) by V_p , we obtain

$$F = \frac{\pi}{3} nm(D+d)^2 v_T V, \quad (2)$$

which agrees well with the simulation results for $V \lesssim v_T$ as shown in Fig. 2. Here, the sound speed is another characteristic speed appeared in this system. However, it is obvious that the thermal speed is superior to the sound speed to characterize the drag law as shown in Appendix A.

III.2. Effect of the boundary conditions on the intruder

In this subsection, let us check how the results depend on the boundary conditions between the intruder and the mobile particles. Here, we refer to the intruder introduced in the previous subsection as (i) “thermal and bumpy”, because the mobile particles reflect at random when they collide with the intruder, and the small particles are attached on the surface of the core particle. We prepare three different types of the intruders: (ii) “reflective and smooth,” (iii) “reflective and bumpy,” and (iv) “thermal and smooth.” The intruder in the condition of (ii) “reflective and smooth” consists of only one core

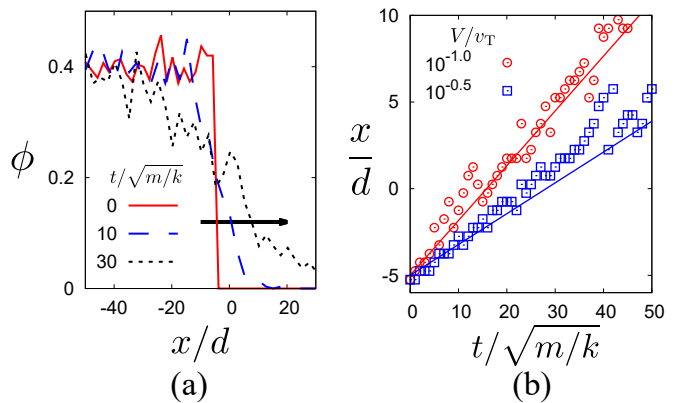


FIG. 4. (a) The time evolution of the density profile at $t/\sqrt{m/k} = 0$ (red solid line), 10 (blue dashed line), and 30 (black dotted line). The arrow indicates the direction of the diffusive front. (b) The expansion wave ($\phi = 0.15$) for $V/v_T = 1.0 \times 10^{-1}$ (open circles) and $1.0 \times 10^{-0.5}$ (open squares). The corresponding solid lines represent the expansion speeds V_p .

particle, and the reflection between the intruder and the mobile particles is elastic. The intruder in (iii) “reflective and bumpy” condition consists of the core particle and the small particles on its surface, where we have used the boundary condition as that used in the first case. The intruder in (iv) “thermal and smooth” condition consists of only one core intruder, where we have used the thermal boundary condition as used in the main text. Figure 5 plots the results of the drag forces under various boundary conditions. The results clearly indicate that the choice of a boundary condition on the intruder is not important for the drag force.

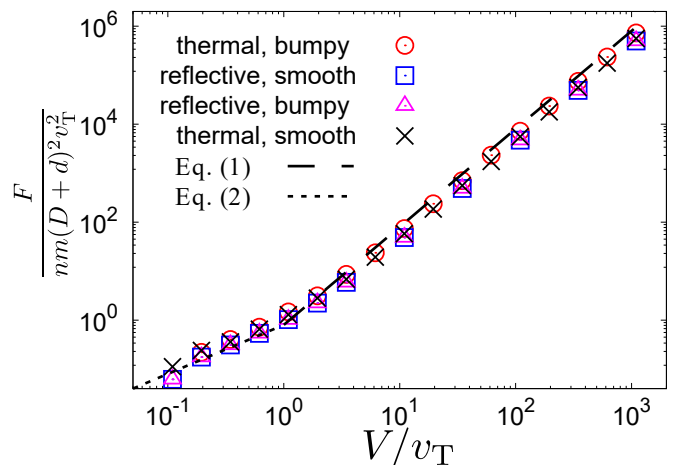


FIG. 5. Plots of the drag force against the scaled collision speed V/v_T for the free scattering case with $\phi = 0.40$ and $D = 7d$ when we examine several reflection rules between the intruder and the mobile particles.

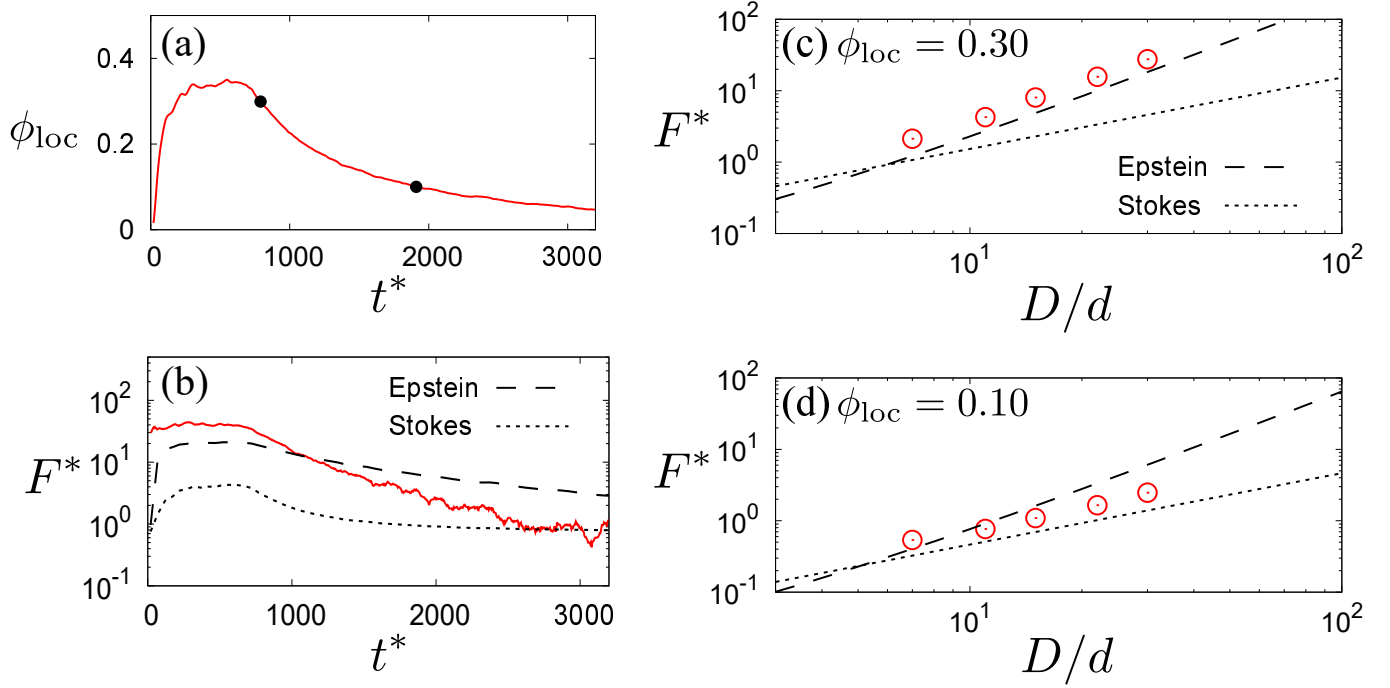


FIG. 6. (a) Time evolution of the local packing fraction ϕ_{loc} in front of the intruder for $\phi = 0.40$, $D/d = 30$, and $V/v_T = 3.2 \times 10^{-1}$. Two black dots represents the points for $\phi_{\text{loc}} = 0.30$ and 0.10 , respectively. (b) Time evolution of the force acting on the intruder. We also plot Epstein's law (2) (dashed line) and Stokes' law (3) (dotted line) using the time evolution of the local packing fraction ϕ_{loc} . (c), (d) The diameter dependence of the force for $\phi_{\text{loc}} = 0.30$ and 0.10 , respectively.

III.3. Crossover from Stokes' law to Epstein's law

In the previous subsection, we have reported the crossover from Epstein's law to Newton's law when we control the ratio of the colliding speed to the thermal speed V/v_T . In this subsection, we fix V/v_T and illustrate the existence of a crossover from Epstein's law to Stokes' law as the time evolution of the drag force acting on the intruder. When we focus on the region in front of the intruder, the packing fraction of this local region changes as time goes on. Figure 6(a) shows the time evolution of this local packing fraction. After the early stage of the collision process, there is relatively long metastable state for the local packing fraction is almost equal to the initial packing fraction of the beam particles. Then, ϕ gradually decreases with time for $t/\sqrt{m/k} > 600$. When we substitute the local packing fraction $\phi_{\text{loc}}(t)$ into Eq. (2), we can observe the crossover from Epstein's drag law to Stokes' drag law as shown in Fig. 6(b). Then, the drag force reaches Stokes' law in the late stage, which is given by

$$F_{\text{St}} = 3\pi\eta DV, \quad (3)$$

where the shear viscosity η is estimated from the well-known result from the Enskog theory [38, 39] as

$$\eta(\phi) = \frac{5}{16d^2} \sqrt{\frac{mT}{\pi}} \times \left[\frac{1}{g_0(\phi)} \left(1 + \frac{8}{5} \phi g_0(\phi) \right)^2 + \frac{768}{25\pi} \phi^2 g_0(\phi) \right]. \quad (4)$$

Here, $g_0(\phi)$ is the radial distribution function at contact, which is approximately given by Carnahan and Starling formula $g_0(\phi) = (1 - \phi/2)/(1 - \phi)^3$ valid for $\phi < 0.49$ [40]. We also confirm that the drag force is proportional to the cross section in Epstein's regime, whereas it is proportional to $D+d$ in Stokes' regime as shown in Figs. 6(c) and (d). This is also another evidence of the crossover from Epstein's law to Stokes' law.

III.4. Flows behind the intruder

Let us characterize the particle flows behind the intruder for large V . We introduce the second invariant of the velocity gradient tensor $Q = (1/2)(-S_{\alpha\beta}S_{\alpha\beta} + W_{\alpha\beta}W_{\alpha\beta})$ where $S_{\alpha\beta} = (1/2)(\partial_\beta u_\alpha + \partial_\alpha u_\beta)$ and $W_{\alpha\beta} = (1/2)(\partial_\beta u_\alpha - \partial_\alpha u_\beta)$ [41]. Here, we adopt Einstein's rule for α and β where duplicated indices take summation over x , y , and z . Figure 7 shows the contour of $Q = 0$, where the field is coarse-grained with the scale $2d$ for visibility [42]. The vortex rich regions $Q > 0$ emerge behind the intruder. This behavior is similar to that observed

in turbulent flows induced by an intruder [7]. We note that the vortex structure also appears when we observe the vorticity (see Appendix B).

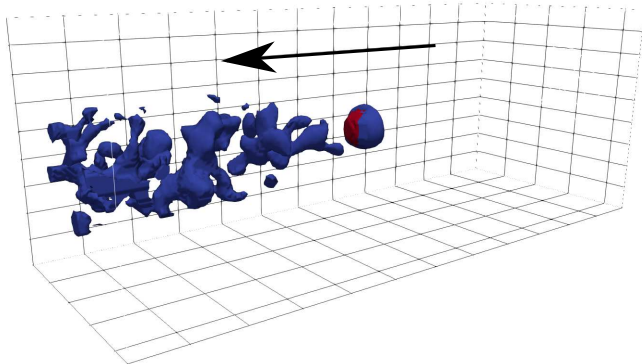


FIG. 7. Contour plot of the second invariant $Q = 0$ for $\phi = 0.40$, $D = 7d$, and $V/v_T = 1.0 \times 10^1$. The arrow indicates the flow direction.

Let us study how the particles are scattered after collisions with the intruder. We focus on the relative motion of the particles which collide with the intruder almost simultaneously through the mean square displacement

$$\Delta(t) \equiv \langle |\delta \mathbf{r}_i(t) - \delta \mathbf{r}_j(t)|^2 \rangle / d^2, \quad (5)$$

with $\delta \mathbf{r}_i(t) \equiv \mathbf{r}_i(t + t_c) - \mathbf{r}_i(t_c)$, where we only select two particles (i and j) within the interval $|t_i - t_j| < \Delta t_{\text{th}} \equiv 10\sqrt{m/k}$ with the collision times t_i and t_j with the intruder for i -th and j -th particles, respectively. Note that t_c in Eq. (5) is larger time of t_i and t_j . Figure 8 shows the super-ballistic behavior $\Delta(t) \sim t^{2.2}$. This behavior is analogous to the relative motion of two tracer particles in turbulent flows, which is known as Richardson's law $\Delta(t) \sim t^3$ [43–45]. We have checked that this result is insensitive to the choice of Δt_{th} in the range $1.0\sqrt{m/k} \lesssim \Delta t_{\text{th}} \lesssim 2.0 \times 10^1 \sqrt{m/k}$. The exponent 2.2 for the super-ballistic $\Delta(t)$ in our system seems to be much smaller than 3 for $\Delta(t)$ in turbulent flows. This is because the fluid flow behind the intruder in our system is not a fully developed turbulence but is a weak turbulence.

Next, we consider the scattering angle distribution of the mobile particles. The azimuthal angle is stored when the particles reach the region $|\mathbf{r}_i| = 15d$. The behavior of the angular distribution $\rho(\theta)$ for $V/v_T \gtrsim 1$ completely differs from that for $V/v_T \lesssim 1$ as shown in Fig. 9. This is also characterized by the coefficients of the Legendre expansion of the angular distribution (see Appendix C).

For $V/v_T \gg 1$, the angular distribution of scattered particles has a sharp peak around the opening angle, which is the half of the apex angle of the cone of the beam scattered after collisions with the intruder [33, 36] as shown in Fig. 10. We also note that this opening angle can be explained by a phenomenology as in Ref. [33]. Because we use repulsive and elastic particles, the opening

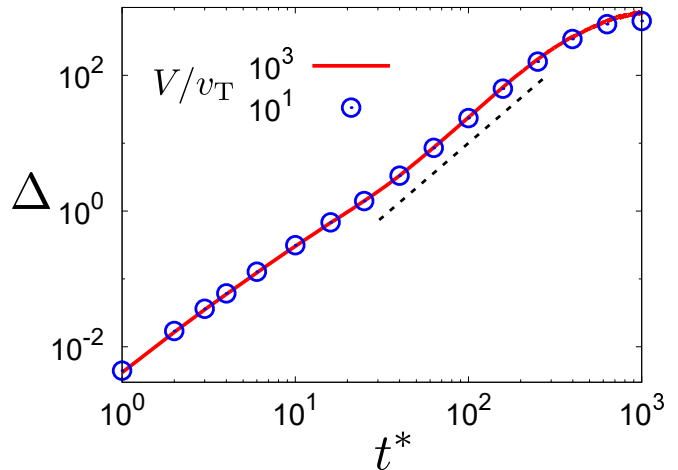


FIG. 8. The mean square displacement between two particles for $V/v_T = 1.0 \times 10^3$ (solid line) and 1.0×10^1 (open circles). The dotted line is the guide line for the exponent 2.2.

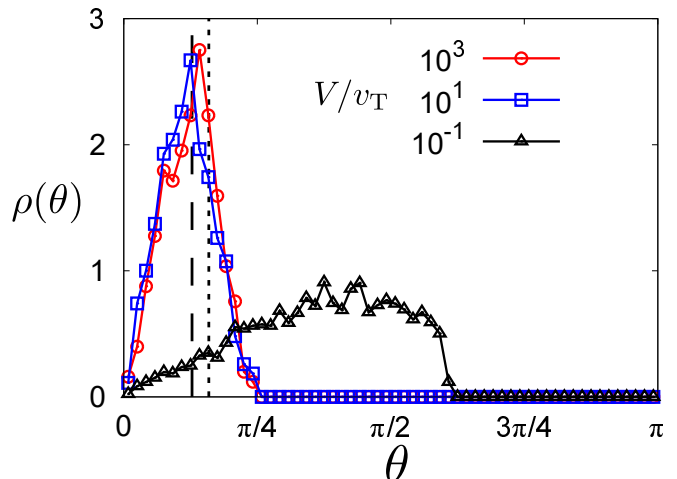


FIG. 9. The angular distribution function of the scattered particles for (a) $V/v_T = 1.0 \times 10^3$ (open circles), (b) 1.0×10^1 (open squares), and (c) 1.0×10^{-1} (open triangles). The dashed and dotted lines represent the opening angles obtained from the simulation and Eq. (6), respectively.

angle is expressed as

$$\theta_0 = \cos^{-1} \left[1 - \left(\frac{D}{2R} \right)^2 \right], \quad (6)$$

for $D < 2R$ [33]. When we substitute $D = 7d$ and $R = 10d$ into Eq. (6), we obtain $\theta_0 = 0.50$ (rad), which roughly agrees with the simulation results (see Fig. 9). For $V/v_T \ll 1$, on the other hand, the particles are scattered in various direction as shown in Fig. 9.

IV. DISCUSSION

Let us discuss our results. We have observed vortex-like structures for large V/v_T in terms of the contour

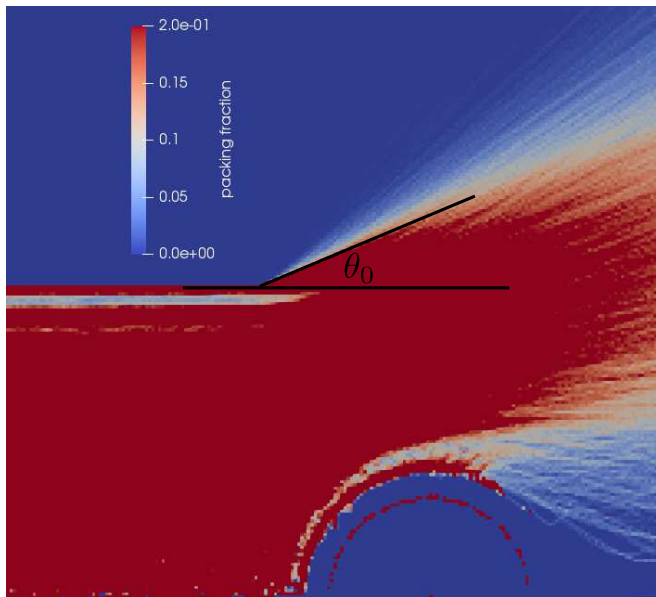


FIG. 10. The definition of the open angle. We choose the opening angle as the direction where the volume fraction is 0.15.

plot of the second invariant $Q = 0$ as shown in Sec. III.4. However, the exponent of the relative diffusion in this regime is much smaller than that for a fully developed turbulence. To observe fully developed turbulences, we need to simulate a larger system where the diameter of the intruder is much larger than that of the surrounding particles, i. e. $D/d \gg 1$. The simulation for such systems will be a future task of our project.

Next, once we will reproduce a crossover from Stokes' flow to fully developed turbulent flows behind the intruder, we will need to characterize the fluid flows in terms of the statistical mechanics of flowing particles. This will be a challenging project to understand the fluid turbulence for $V/v_T \gg 1$ based on statistical mechanics.

V. CONCLUSION

We have numerically studied the particle flows injected as a beam and scattered by a spherical intruder. We have found the crossover from Epstein's law to Newton's law, depending on the ratio of the speed to the thermal speed V/v_T . This crossover can be explained by a simple collision model. The crossover from Epstein's law to Stokes' law is also verified as the time evolution of the drag force acting on the intruder. The weak turbulent-like behavior has been also observed for $V/v_T \gg 1$, where the mean square displacement is weakly super-ballistic. The scattering of particles by the intruder is also characterized by the angular distribution function of scattered particles.

ACKNOWLEDGMENTS

The authors thank Hiroshi Watanabe, Kuniyasu Saitoh, Takeshi Kawasaki, and Michio Otsuki for their useful comments. Numerical computation in this work was partially carried out at the Yukawa Institute Computer Facility. This work is partially supported by Scientific Grant-in-Aid of Japan Society for the Promotion of Science, KAKENHI (Grant No. 16H04025) and the YITP activities (Grant No. YITP-T-18-03 and No. YITP-W-18-17).

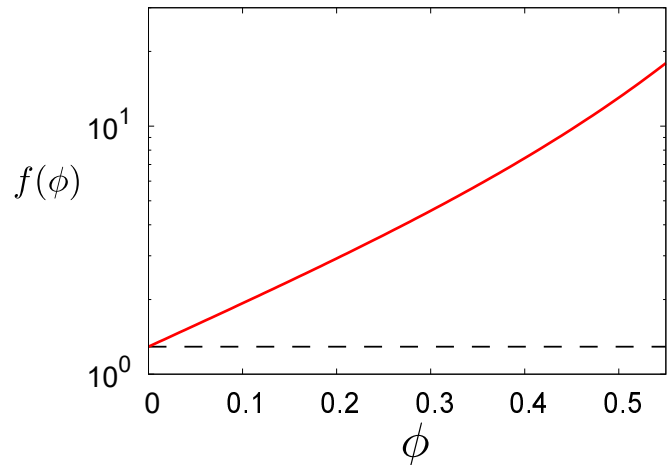


FIG. 11. Plot of $f(\phi)$ as a function of the volume fraction. The dashed line shows $\sqrt{5/3}$, which is the coefficient for the ideal gas.

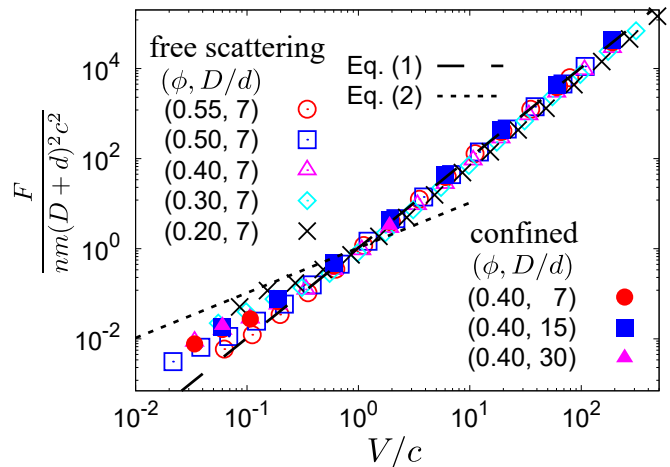


FIG. 12. Plots of the drag force against the dimensionless velocity characterized by the sound speed (A4) for free scattering and confined cases for various ϕ and intruder sizes D . The dashed and dotted lines represent the collision model (1) and (2) with the expansion speed $V_p' = \sqrt{c(\phi)V}$, respectively.

Appendix A: Volume fraction dependence of the sound speed

In this Appendix, we show how the sound speed depends on the volume fraction. We also examine whether v_T can be replaced by the sound speed.

Because the volume fraction of the mobile particles is finite, the equation of state deviates from that for the ideal gas. Thus, the equation of state at finite density is fitted by the Carnahan-Starling equation [40]

$$\frac{p}{nT} = Z(\phi) = \frac{1 + \phi + \phi^2 - \phi^3}{(1 - \phi)^3}, \quad (\text{A1})$$

where p is the static pressure. For the adiabatic process, the first law of thermodynamics becomes

$$C_V dT + T \left(\frac{\partial p}{\partial T} \right)_V \frac{dL^3}{N} = 0, \quad (\text{A2})$$

where L^3 is the volume, $C_V = 3/2$ is the heat capacity at constant volume. Substituting the equation of state (A1), the following quantity is conserved:

$$\log \frac{p}{\phi Z(\phi)} - \frac{2}{3} \int^\phi \frac{Z(\phi')}{\phi'} d\phi' = \text{const.} \quad (\text{A3})$$

Then, the sound speed in the adiabatic process is given by

$$c(\phi) = \sqrt{\left(\frac{\partial p}{\partial \rho} \right)_S} = f(\phi) \sqrt{\frac{T}{m}}, \quad (\text{A4})$$

with

$$f(\phi) = \sqrt{\frac{5 + 10\phi - 3\phi^2 - 24\phi^3 + 37\phi^4 - 22\phi^5 + 5\phi^6}{3(1 - \phi)^6}}. \quad (\text{A5})$$

Figure 11 shows the volume fraction dependence of the coefficient $f(\phi)$. If we adopt the expansion speed $V_p' = \sqrt{c(\phi)V}$, the drag force for the low V/c cannot be captured as shown in Fig. 12.

Appendix B: Vorticity

In this Appendix, we also characterize the vortex structure by plotting the vorticity induced by the scattering of the intruder. In the following, we choose z -axis as the flow direction. Because the twisted structure of the flow field is not observed in our simulation, we focus on the flow structure in xz -plane. Let us introduce the vorticity in xz -plane with $|y_i| \leq D/2$ as

$$\omega_{xz} = \frac{\partial v_z}{\partial x} - \frac{\partial v_x}{\partial z}. \quad (\text{B1})$$

Figure 13 shows a typical snapshot of the vorticity field in xz -plane. The positive and negative vorticity regimes are generated in the vicinity of the intruder and move toward the downstream. (See the movie in the Supplemental Material [46].)

Appendix C: Legendre expansion of scattered particles

In this Appendix, we analyze the azimuthal angular distribution discussed in Sec. III.4. Let us expand the distribution $\rho(\theta)$ in terms of the Legendre polynomials as

$$\rho(\theta) = \sum_{\ell=0}^{\infty} A_\ell P_\ell(\cos \theta), \quad (\text{C1})$$

where $P_\ell(x)$ is the Legendre polynomial of degree ℓ [47], and A_ℓ is the coefficient defined by

$$A_\ell = \frac{2\ell + 1}{2} \int_{-1}^1 \rho(\theta) P_\ell(\cos \theta) d \cos \theta. \quad (\text{C2})$$

Figure 14 shows the coefficient for each degree ℓ . The coefficients converge slowly to zero for large ℓ . For $V/v_T \gg 1$, A_ℓ has a peak at $\ell = 2$, while the behavior is different for small V/v_T .

-
- [1] S. H. Lamb, *Hydrodynamics*, Dover, New York (1945).
[2] G. K. Batchelor, *An introduction to fluid dynamics*, Cambridge Univ. Press, Cambridge (1967).
[3] M. Vergeles, P. Koblinski, J. Koplik, and J. R. Banavar, Phys. Rev. Lett. **75**, 232 (1995), Phys. Rev. E **53**, 4852 (1996).
[4] S. Chen, N. Phan-Thien, B. C. Khoo, and X. J. Fan, Phys. Fluids **18**, 103605 (2006).
[5] Z. Li and G. Drazer, Phys. Fluids **20**, 103601 (2008).
[6] M. Itami and S. Sasa, J. Stat. Phys. **161**, 532 (2015).
[7] Y. Asano, H. Watanabe, and H. Noguchi, J. Chem. Phys. **148**, 144901 (2018).
[8] E. Cunningham, Proc. R. Soc. A **83**, 357 (1910).
[9] M. Knudsen and S. Weber, Ann. Phys. **36**, 981 (1911).
[10] Y. Sone, *Molecular Gas Dynamics: Theory, Techniques, and Applications* (Birkhauser, Boston, 2007).
[11] S. Takata, Y. Sone, and K. Aoki, Phys. Fluids A **5**, 716 (1993).
[12] S. Taguchi, J. Fluid Mech. **774**, 363 (2015).
[13] S. Taguchi and T. Suzuki, Phys. Rev. Fluids **2**, 113401 (2017).
[14] P. S. Epstein, Phys. Rev. **23**, 710 (1924).
[15] Z. Li and H. Wang, Phys. Rev. E **68**, 061206 (2003).
[16] H. Brenner, Chem. Eng. Sci. **16**, 242 (1961).
[17] D. C. Rapaport and E. Clementi, Phys. Rev. Lett. **57**, 695 (1986).
[18] T. S. Komatsu, S. Matsumoto, T. Shimada, and N. Ito, Int. J. Mod. Phys. C **25**, 1450034 (2014).

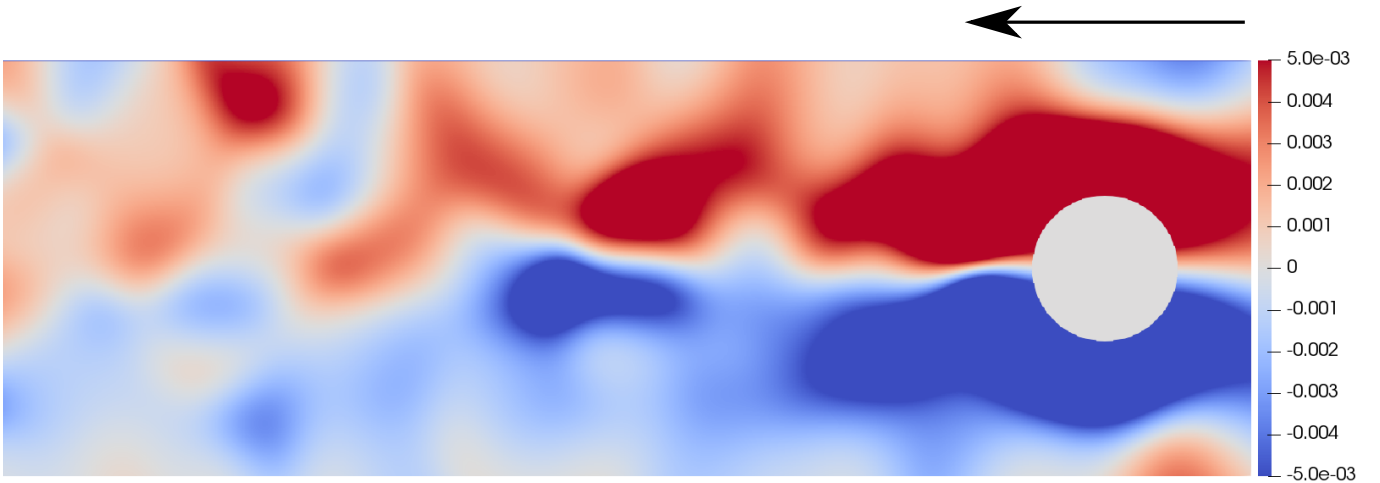


FIG. 13. Vorticity field behind the intruder for $V/v_T = 1.0 \times 10^3$. The color represents the value of $\omega_{xz}/\omega_{\max}$ with $\omega_{\max} = 5.0 \times 10^{-3} (k/m)^{1/2}$. The arrow indicates the flow direction.

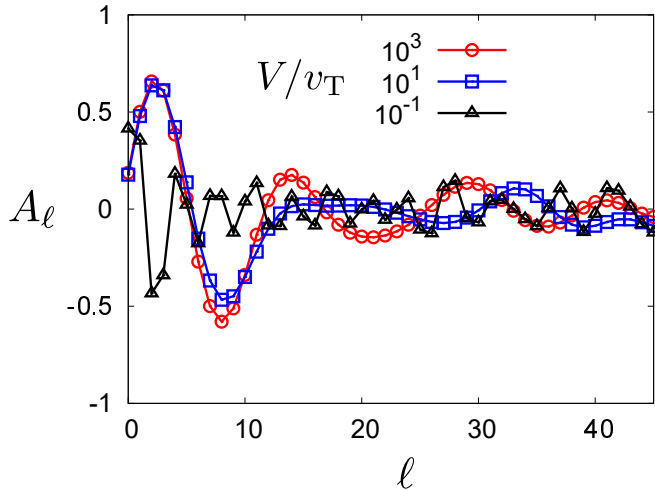


FIG. 14. The coefficients of the Legendre expansion of the angular distribution function for (a) $V/v_T = 1.0 \times 10^3$ (open circles), (b) 1.0×10^1 (open squares), and (c) 1.0×10^{-1} (open triangles).

[19] R. Albert, M. A. Pfeifer, A.-L. Barabási, and P. Schiffer, Phys. Rev. Lett. **82**, 205 (1999), I. Albert, P. Tegzes, R. Albert, J. G. Sample, A.-L. Barabási, T. Vicsek, B. Kahng, and P. Schiffer, Phys. Rev. E **64**, 031307 (2001).
 [20] D. Chehata and R. Zenit, Phys. Fluids **15**, 1622 (2003).
 [21] C. R. Wassgren and J. A. Cordova, Phys. Fluids **15**, 3318 (2003).
 [22] J. Geng and R. P. Behringer, Phys. Rev. Lett. **93**, 238002 (2004), Phys. Rev. E **71**, 011302 (2005).
 [23] R. Bharadwaj and C. Wassgren, Phys. Fluids **18**, 043301 (2006).
 [24] F. Q. Potiguar and Y. Ding, Phys. Rev. E **88**, 012204 (2013).
 [25] Y. Takehara, S. Fujimoto, and K. Okumura, EPL **92**, 44003 (2010), Y. Takehara and K. Okumura, Phys. Rev. Lett. **112**, 148001 (2014).

[26] K. A. Reddy, Y. Forterre, and O. Pouliquen, Phys. Rev. Lett. **106**, 108301 (2011).
 [27] J. E. Hilton and A. Tordesillas, Phys. Rev. E **88**, 062203 (2013).
 [28] F. Guillard, Y. Forterre, and O. Pouliquen, Phys. Rev. Lett. **110**, 138303 (2013), Phys. Rev. E **91**, 022201 (2015).
 [29] S. Takada and H. Hayakawa, J. Eng. Mech. **143**, C4016004 (2017).
 [30] R. Candelier and O. Dauchot, Phys. Rev. E **81**, 011304 (2010).
 [31] M. V. Gnann, I. Gazuz, A. M. Puertas, M. Fuchs, and T. Voigtmann, Soft Matter **7**, 1390 (2011).
 [32] T. Wang, M. Grob, A. Zippelius, and M. Sperl, Phys. Rev. E **89**, 042209 (2014), D. Wang, Y. Yang, and W. Du, Powder Technol. **286**, 385 (2015).
 [33] X. Cheng, G. Varas, D. Citron, H. M. Jaeger, and S. R. Nagel, Phys. Rev. Lett. **99**, 188001 (2007), X. Cheng, L. Gordillo, W. W. Zhang, H. M. Jaeger, and S. R. Nagel, Phys. Rev. E **89**, 042201 (2014).
 [34] J. Ellowitz, H. Turler, N. Guttenberg, W. W. Zhang, and S. R. Nagel, Phys. Rev. Lett. **111**, 168001 (2013).
 [35] P. Müller, A. Formella, and T. Pöschel, J. Fluid Mech. **751**, 601 (2014).
 [36] T. G. Sano and H. Hayakawa, Phys. Rev. E **86**, 041308 (2012), Prog. Theor. Exp. Phys. **2013**, 103J02 (2013).
 [37] S. Takada and H. Hayakawa, arXiv:1901.02255 (to appear in Granular Matter).
 [38] J. Ferziger and H. Kaper, *Mathematical Theory of Transport Processes in Gases* (North-Holland, Amsterdam, 1972).
 [39] V. Garzó and J. W. Dufty, Phys. Rev. E **59**, 5895 (1999).
 [40] N. F. Carnahan and K. E. Starling, J. Chem. Phys. **51**, 635 (1969).
 [41] J. C. R. Hunt, A. A. Wray, and P. Moin, Center for Turbulence Research Report CTR-S88, 1988.
 [42] J. Zhang, R. P. Behringer, and I. Goldhirsch, Prog. Theor. Phys. Suppl. **184**, 1 (2010).
 [43] L. F. Richardson, Proc. R. Soc. London A **110**, 709 (1926).

- [44] A. Monin and A. Yaglom, *Statistical Fluid Mechanics* (MIT Press, Cambridge, MA, 1975), Vol. 2.
- [45] G. Boffetta and I. M. Sokolov, Phys. Rev. Lett. **88**, 094501 (2002).
- [46] See the ancillary file for the movie for $V/v_T = 1.0 \times 10^3$.
- [47] M. Abramowitz and I. A. Stegun, *Handbook of Mathematical Functions: With Formulas, Graphs, and Mathematical Tables* (Dover, New York, 1964).